Spectroscopic Characterization of Highly Dispersed Vanadia Supported on SBA-15

Christian Hess,[†,§] James D. Hoefelmeyer,[†] and T. Don Tilley*[,†,‡]

Department of Chemistry, University of California, Berkeley, Berkeley, California 94720-1460, and the Chemical and Materials Science Divisions, Lawrence Berkeley National Laboratory, 1 Cyclotron Road, Berkeley, California 94720

Received: December 4, 2003; In Final Form: April 28, 2004

Spectroscopic analysis was used to gain new insight into the molecular structures occurring during the synthesis of highly dispersed silica SBA-15 supported vanadia (VO_x/SBA-15). VO_x/SBA-15 was prepared by a grafting/anion-exchange procedure. As a first step of the procedure, the inner pores of SBA-15 are functionalized via grafting of 3-aminopropyltrimethoxysilane. After formation of the corresponding ammonium salt, decavanadate ($V_{10}O_{28}^{6-}$) is incorporated into the pores by anion exchange. In the final step, calcination of the decavanadate precursor, yields the chemically bonded vanadia species. Using this approach, vanadium loadings of up to 22 wt % of V on SBA-15 were obtained. As followed by Raman spectroscopy, upon dehydration, the structure of the supported vanadia changes dramatically. Raman and diffuse reflectance UV−vis spectroscopy under dehydrated conditions reveal the presence of different vanadia structures (monomers, polymers, and crystals) as a function of vanadium loading (0−22 wt % of V). The maximum coverage of vanadia species on SBA-15 is achieved at ∼7.2 wt % of V (2.3 V/nm^2). At loadings up to 7.2 wt % of V, the vanadia species are mainly present as isolated tetrahedral species, whereas at higher loadings V_2O_5 crystallites are formed, in addition to monomeric and polymeric vanadia species.

Introduction

SBA-15 is a purely siliceous mesoporous molecular sieve with uniform hexagonal channels ranging from 5 to 30 nm and having a very narrow pore size distribution.[1] It is a promising new support material for catalysts as its thick framework walls (3.1−6.4 nm) provide high hydrothermal stability that exceeds those of the thinner-walled MCM-41 materials.[1−3] In addition, its large internal surface area (>800 m^2/g) allows for the dispersion of a large number of catalytically active centers. Although of great potential use for catalytic applications, there have been only a few reports on the modification of SBA-15 with vanadium oxides using various impregnation techniques.[4,5] Despite these efforts, a thorough investigation of the structural properties of VO_x/SBA-15 as a function of vanadium loading is still missing.

Grafting methods are widely used to prepare catalysts on support materials. In a previous study, 3-aminopropyltrimethoxysilane (APTMS) has been used as a linker to attach iron and copper species to the surface of MCM-41.[6] Recently, by using molecular designed dispersion (MDD) of $VO(acac)_2$, highly dispersed VO_x species have been grafted onto MCM-48.[7] We have developed a grafting/anion exchange method to anchor transition metal oxides onto high surface area supports. This method consists of (1) functionalization of the inner pores of SBA-15 with 3-aminopropyltrimethoxysilane followed by protonation with aqueous HCl, (2) ion-exchange of the precursor (decavanadate in this study) into the pores, and (3) decomposition of the precursor yielding a highly dispersed, supported transition metal oxide catalyst.

The grafting/anion exchange method offers several advantages. The inner pores are functionalized with propylammonium chloride groups. The highly charged decavanadate anion is introduced as the vanadium source. Decavanadate can potentially exchange for six chloride anions, resulting in an entropic driving force for the anion exchange. The precursor is tightly held electrostatically within the channels, and does not leach into aqueous solution. This method allows the precise control over the amount of vanadium introduced into the material up to a maximum vanadium content of 22 wt %. The immobilized decavanadate precursor is thermally decomposed to yield supported VO_x/SBA-15 materials that are thermally stable to 550 °C.

Vanadium oxides supported on amorphous silica have received much attention in recent years because of their catalytic and structural properties. They exhibit high activity and selectivity for a number of oxidation reactions, such as the partial oxidation of methane,[8,9] methanol oxidation to formaldehyde,[10−12] and the oxidative dehydrogenation of ethane to ethylene.[13] Previous studies have shown that the catalytic performance of supported vanadia catalysts crucially depends on the structure and distribution of the dispersed surface vanadium oxide species. To understand the relationship between structural and catalytic properties of dispersed vanadia, various techniques including infrared,[14−16b] Raman,[17−21] UV−visible,[14,15,18,22,23] solid-state ^{51}V NMR,[19] and X-ray absorption spectroscopy[16,24] have been used. It is generally accepted that, in the absence of water, at low vanadia loadings (<5 wt % of V_2O_5) the surface vanadium oxide species are isolated VO_4 units. At high loadings (although well below those required for a monolayer of polymeric vanadia) crystalline V_2O_5 is formed. However, controversy exists over the types of vanadium oxide species at intermediate vanadia loadings. On the basis of diffuse reflectance UV−vis and Raman data, Wokaun et al. proposed the presence of monomers/

* To whom the correspondence should be addressed. E-mail: tdtilley@socrates.berkeley.edu.

† Lawrence Berkeley National Laboratory.

‡ University of California, Berkeley.

§ Present address: Abteilung Anorganische Chemie, Fritz-Haber-Institut der Max-Planck-Gesellschaft, Faradayweg 4-6, D-14195.

10.1021/jp037714r CCC: $27.50
Published on Web 06/05/2004

polymers with a VO_4 coordination geometry as well as ribbons with a square pyramidal coordination geometry.[15] On the basis of their diffuse reflectance UV−vis results, Johnson et al. suggest that polyvanadium chains are present.[14] Using the same technique, Arena et al. proposed the presence of di- and oligomeric VO_4 structures on the 5 wt % of V_2O_5/SiO_2 catalyst and 2D patches of pentacoordinated vanadium on the 20 wt % of V_2O_5/SiO_2 catalyst.[23] Inumaru et al. proposed the formation of thin vanadia overlayers, which contain V−O−V bonds, for their VO_x/SiO_2 samples prepared by CVD (chemical vapor deposition).[16] In contrast, based on results from ^{51}V NMR and Raman spectroscopy as well as UV−vis and XANES spectroscopies, Wachs et al. concluded that only isolated VO_4 species were present on a silica surface, even at a high loading of 10 wt % of V_2O_5.[18,19]

In this contribution we discuss the synthesis of highly dispersed surface vanadia species by functionalization of SBA-15 and subsequent anion exchange using butylammonium decavanadate followed by thermolysis. Raman and UV−vis diffuse reflectance spectroscopy are used to elucidate the structure of the supported VO_x phase during synthesis and after dehydration.

Experimental Section

1. Catalyst Preparation. *SBA-15.* Silica SBA-15 was synthesized according to the literature.[1] Briefly, 4.0 g of Pluronic P-123 was combined with 120 mL of 2 M HCl and 30 mL of deionized water in a polypropylene bottle and stirred to 35 °C until it was completely dissolved. To this solution was added 8.5 g of TEOS under rigorous stirring. The contents were stirred for 20 h at 35 °C, then placed in an oven at 85 °C for 24 h. The white product was filtered over a glass frit and washed with acetone, resulting in a white powder. The powder was calcined at 550 °C in air for 12 h to obtain the final product.

Ammonium-Functionalized SBA-15. To a suspension of 2.5 g of SBA-15 in 100 mL of toluene at 65 °C was added 6.5 g of 3-aminopropyltrimethoxysilane (APTMS) with stirring. After being stirred for 12 h, the contents were filtered and washed with toluene to remove any free amine. This dry, white powder was stirred in 150 mL of 0.3 M HCl for 12 h. The contents were filtered again, washed with water, and dried in air overnight, yielding 4.8 g of white powder. Elemental analysis (UCB Microlab) indicated a carbon content of 11.33% and a nitrogen content of 3.55% for a sample dried for 12 h in air at 85 °C. Based on an original SBA-15 sample of 826 m^2/g, the nitrogen content corresponds to 2.66 mmol N/g and thus a loading of 1.94 N/nm^2. This value is in very good agreement with results obtained in other studies.[25]

Butylammonium Decavanadate. Butylammonium decavanadate was synthesized according to a previous report.[26] In a 250-mL flask with a reflux condenser, 5 g of V_2O_5 and 2.41 g of butylamine were added to 100 mL of water. The reaction mixture was heated until the contents were completely dissolved. The solution pH was adjusted to 6 by dropwise addition of concentrated $HClO_4$. The deep orange solution was refluxed overnight. The mixture was filtered, and water was removed by evaporation, leaving a brilliant orange powder. The powder is highly soluble in water and can be recrystallized from acetone/water ~10:1 (v/v).

VO_x/SBA-15. SBA-15-supported vanadia was synthesized with use of functionalized SBA-15 and butylammonium decavanadate as starting materials. For a 2.3 wt % of V catalyst, 73 mg of butylammonium decavanadate was added to a suspension of 1 g of functionalized SBA-15 in 40 mL of water. The contents were stirred for 12 h, filtered, washed with water, and dried in air, yielding an orange powder. The powder was calcined at 550 °C for 12 h.

TABLE 1: Surface and Porosity Characteristics of VO_x/SBA-15 Compared with SBA-15

	V (wt %)	V (mmol/g)	V (nm^2)	S_{BET} (m^2/g)	r_p (nm)	V_p (mL/g)
blank SBA-15	0	0	0	826	3.58	0.77
VO_x/SBA-15	2.3	0.45	0.61	445	3.26	0.46
	4.3	0.83	0.88	442	3.09	0.4
	7.2	1.41	2.3	369	2.83	0.36
	9	1.77	6.74	158	2.89	0.32
	18.3	3.58	28	76	1.97	0.23
	21.9	4.31	36	72	2.82	0.3

2. Physical Characterization. The vanadium content of the VO_x/SBA-15 samples was determined by Galbraith Laboratories, Inc., Knoxville, TN.

Surface areas of the prepared samples were measured by nitrogen adsorption/desorption isotherms, using a Quantachrome Instruments Autosorb-1 surface area analyzer and standard multipoint BET[27] analysis methods. The pore volume was determined from the adsorption branch of the N_2 isotherm curve at the $P/P_0 = 0.995$ signal point. The pore-size distribution was calculated from the desorption branch of the isotherm, using the BJH[28] method.

3. Raman Spectroscopy. The Raman spectrometer (Kaiser Optical) was equipped with a Nd:YAG laser that is frequency doubled to 532 nm. The laser was operated at a power level of 25 mW measured at the sample with a power meter (Coherent). The spectral resolution of the spectrometer is 5 cm^{-1}. To minimize the effect of laser heating the samples (~50 mg) were pressed into pellets at 40 MPa and rotated at 20 Hz within a rotary quartz Raman cell. Sampling times were between 100 and 200 s. The Raman spectra of the dehydrated vanadia samples were recorded at room temperature after heating the samples in flowing air at 400 °C for 1 h.

4. UV−Vis Diffuse Reflectance Spectroscopy. Diffuse reflectance UV−vis spectra were measured with a Varian-Cary 4 spectrometer equipped with a Harrick diffuse reflectance attachment. Samples were dehydrated in 20% O_2/He at 300 °C for 1 h before spectra at ambient temperature between 1 and 5 eV were measured. The Kubelka−Munk function ($F(R_\infty)$) was used to convert diffuse reflectance data into absorption spectra, using MgO as a standard.

Results and Discussion

1. The Synthesis of VO_x/SBA-15. *Physical Characterization.* The synthesis and characterization of pure SBA-15 has been discussed previously.[1] The results of the physisorption characterization of the SBA-15 and VO_x/SBA-15 (0−22 wt % of V) samples are given in Table 1. As indicated by X-ray diffraction and TEM, the hexagonal structure of SBA-15 is preserved in the presence of vanadia. With increasing vanadia loading, the surface area, pore radius, and pore volume of the VO_x/SBA-15 shift to lower values (see Table 1). However, BET also reveals that in the presence of vanadium oxide the mesoporous channels remain accessible. The pore radius and pore volume decrease significantly with loading, which suggests that the vanadia species are located inside the pores of SBA-15, coating the inner walls of the mesoporous matrix. At higher loadings (>7.2 wt % of V), a strong decrease in surface area is observed. As discussed below, Raman spectroscopy reveals that above 7.2 wt % of V, 3-dimensional V_2O_5 crystallites are present. The

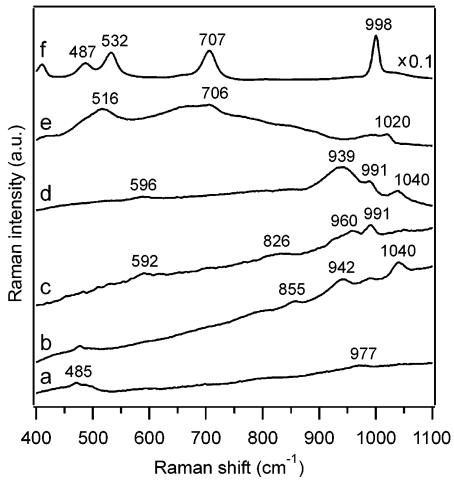

Figure 1. Raman spectra (a) of the blank SBA-15, (b) after reaction of SBA-15 with APTMS, (c) of butylammonium decavanadate, (d) after ion exchange with decavanadate, (e) after calcination in air at 550 °C, and (f) of crystalline V_2O_5. The spectra are offset for clarity.

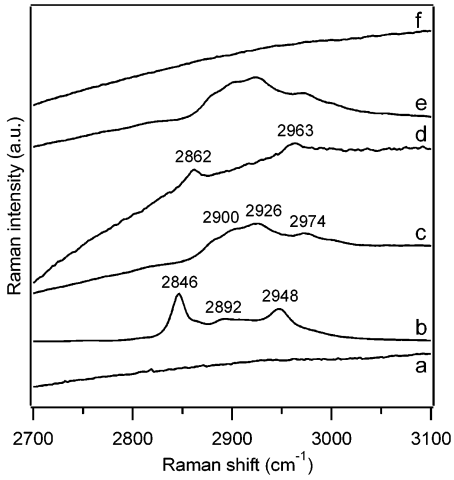

Figure 2. Raman spectra (a) of the blank SBA-15, (b) of the APTMS precursor, (c) after reaction of SBA-15 with APTMS, (d) of methoxy on SBA-15, (e) after ion exchange with decavanadate, and (f) after calcination in air at 550 °C. The spectra are offset for clarity.

smaller surface areas at higher loadings may therefore be caused by channel blocking.

Spectroscopic Characterization. The synthesis of the VO_x/SBA-15 samples was monitored with visible Raman spectroscopy. The following discussion focuses on the preparation of a sample with a loading of 7.2 wt % of V (2.3 V/nm^2). Similar results were obtained for samples with lower vanadia loading (4.3 wt % of V). In the following, the low-frequency (Figure 1) and high-frequency region (Figure 2) of the Raman spectra will be discussed separately. They were recorded at room temperature under ambient conditions.

Figure 1 shows a series of low-frequency Raman spectra obtained during the synthesis of 7.2 wt % (V) of VO_x/SBA-15. The spectrum of blank SBA-15 (spectrum a) shows Raman features around 485 and 977 cm^{-1}, which can be assigned to cyclic tetrasiloxane rings of the silica support (D1 defect mode)[29] and the Si−OH stretch of surface hydroxyl groups,[30] respectively. Weaker Raman bands appear at ∼600 and ∼810 cm^{-1}. They are attributed to cyclic trisiloxane rings (D2 defect mode) and the symmetrical Si−O−Si stretching mode, respectively.[29] Functionalization of SBA-15 with APTMS and subsequent transformation into the ammonium salt leads to the appearance of new bands at 855, 942, and 1040 cm^{-1} (see spectrum b), which are assigned to C−C stretch vibrations of the propylammonium group.[31] Spectrum c corresponds to the as-synthesized butylammonium decavanadate $[H_3NC_4H_9]_6V_{10}O_{28}$ precursor. The presence of Raman bands at 592, 826, 960, and 991 cm^{-1} is in agreement with those reported for sodium decavanadate ($Na_6V_{10}O_{28}\cdot 18H_2O$).[32] After ion exchange of decavanadate into the pores of SBA-15, spectrum d is obtained, which is characterized by Raman bands at 596, 939, 991, and 1040 cm^{-1}. Qualitatively, spectrum d can be considered as a superposition of spectra b and c as, based on the high-frequency region of the Raman spectra, the functionalized SBA-15 is unaffected by the anion exchange (see below). After thermal decomposition of the decavanadate precursor, spectrum e is obtained, which shows Raman bands at 516, 654, 706, 988, and 1020 cm^{-1}. Their similarity with the Raman bands of V_2O_5 crystallites (spectrum f) suggests a V_2O_5-like structure. Previously, similar bands have been observed on amorphous silica.[17,18] They were assigned to hydrated surface vanadium oxide species forming a $V_2O_5\cdot nH_2O$ gel.[33]

Figure 2 depicts the high-frequency region of Raman spectra obtained during the synthesis of 7.2 wt % (V) of VO_x/SBA-15. As reference, the spectra of blank SBA-15 (spectrum a) and neat 3-aminopropyltrimethoxysilane (APTMS, spectrum b) are shown. The spectrum of APTMS shows Raman bands at 2846, 2892, 2948, and 2986 (sh) cm^{-1}. The 2892-cm^{-1} Raman feature is attributed to CH_2 asymmetric stretching. The bands at 2846 and 2948 cm^{-1} are characteristic of the C−H symmetric stretching vibrations, and the shoulder at 2986 cm^{-1} is characteristic of the C−H asymmetric stretching vibration of a methoxy group. The latter three bands were the only bands observed for neat tetramethoxysilane (not shown). Note that the C−H symmetric stretching vibrations of methoxy on SBA-15 (spectrum d) are blue shifted by ∼15 cm^{-1} compared to neat APTMS (spectrum b). Methoxy groups which have not reacted during functionalization and/or polymerization of APTMS would therefore give rise to Raman bands around 2862 and 2963 cm^{-1}. After grafting of APTMS onto SBA-15 and subsequent formation of the ammonium salt spectrum c was obtained. No methoxy-related Raman bands are observed in spectrum c, which suggests that a large fraction of the methoxy groups of APTMS has reacted. Spectrum c shows bands at ∼2900, 2926, and 2974 cm^{-1}, which are attributed to CH_2 asymmetric and NH_3^+ symmetric stretching vibrations, respectively. The latter assignment has been confirmed by comparison with the Raman spectrum of butylammonium chloride, which gives rise to a peak at 2971 cm^{-1}. The ion exchange of decavanadate for chloride does not affect the high-frequency region of the spectrum (see spectrum d). After the final step of the synthesis, the thermal decomposition of decavanadate, and formation of VO_x/SBA-15, no high-frequency Raman bands were observed (see spectrum f). The absence of CH_x- and NH_3^+-related stretching bands suggests that a large portion if not all of the grafted ammoniumpropyl is removed during the thermal treatment.

2. Reaction Mechanism of VO_x/SBA-15 Formation. On the basis of these results the formation of VO_x/SBA-15 can be summarized as follows (Scheme 1): (1) SBA-15 is modified by grafting of 3-aminopropyltrimethoxysilane and subsequent formation of the corresponding ammonium salt. As has been shown previously for 3-aminopropyltriethoxysilane (APTS), after hydrolysis both bidentate and tridentate (polymerized) APTS molecules are present.[34,35] (2) Decavanadate ($V_{10}O_{28}^{6-}$) is incorporated into the pores by using anion exchange, without any indication of structural changes, as evidenced by Raman spectroscopy. (3) Calcination of the decavanadate precursor

SCHEME 1: Functionalization of the Surface of SBA-15 Is Followed by Anion Exchange[a]

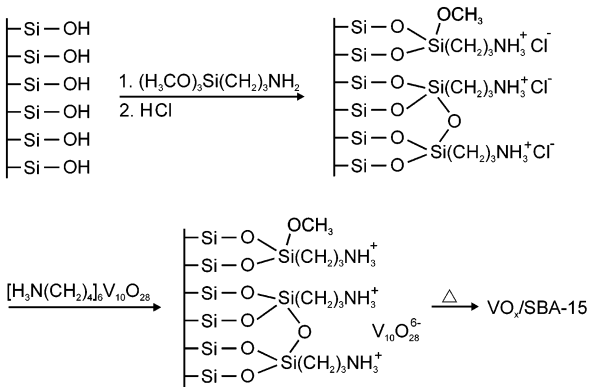

[a] Subsequent calcination yields the final supported oxide material, VO_x/SBA-15.

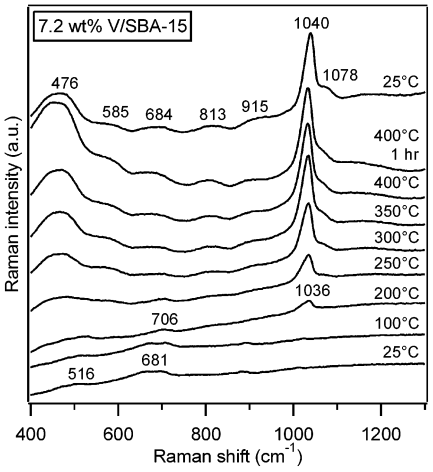

Figure 3. Raman spectra of 7.2 wt % of VO_x/SBA-15 during dehydration in flowing air. The top spectrum was obtained after cooling the sample from 400 to 25 °C. The spectra are offset for clarity.

yields the chemically bonded vanadia species. During this process, previously grafted propylammonium is removed from the pores.

3. Dehydration of VO_x/SBA-15. It is known that the presence of water can influence the structure of dispersed vanadia species. Figure 3 shows a series of Raman spectra, which were obtained while the temperature of the vanadia sample (7.2 wt % of V) was raised to 400 °C in air (100 mL/min) at 10 deg/min. The room-temperature spectrum (shown at the bottom) was recorded before the air flow was initiated. It possesses broad Raman bands around 516, 681, and 1018 cm^{-1}, which are characteristic of hydrated VO_x/SBA-15. It has been noted that hydrated monolayers of VO_x/SBA-15 adopt a gel-like structure that consists of interwoven two-dimensional vanadia ribbons in which vanadium is surrounded by five oxygen ligands forming a square pyramid.[33] Heating the sample in flowing air leads to significant changes in the spectra. The bands around 516 and 681 cm^{-1} become weaker and new Raman bands appear around 480, 585, 680, 810, 915, 1035, and 1074 cm^{-1}. At higher temperatures the features at ~480 and 1035 cm^{-1} dominate the spectra, while broad, weak features at ~585, 684, 813, and 915 cm^{-1} remain visible. The broad 480-cm^{-1} band is assigned to the D1 defect mode (see above). It results from condensation of surface hydroxyls upon heating. The Raman spectrum of dehydrated VO_x/SBA-15 exhibits similarities to the model complex, $OV[OSi(O^tBu)_3]_3$,[36] although the intensity of several bands is diminished. The weak feature centered at 684 cm^{-1} may be

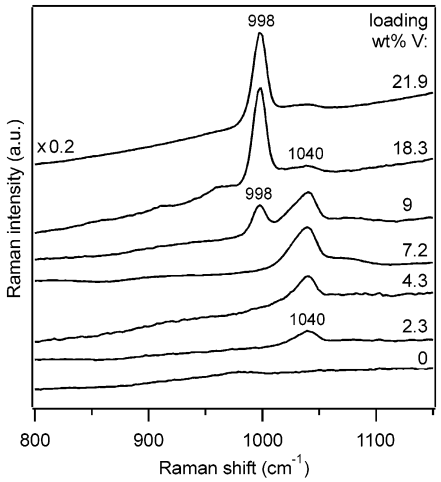

Figure 4. Raman spectra of dehydrated SBA-15-supported vanadia samples. The spectra are offset for clarity.

TABLE 2: Comparison between the Spectral Features and the Inferred Structures of VO_x/SBA-15 Samples

V (wt %)	*V* (nm^2)	Raman features (cm^{-1})	UV−vis abs max (nm)	VO_x structure
2.3	0.61	1040	254	T_d, mono
4.3	0.88	1040	260	T_d, mono
7.2	2.3	1040	266	T_d, mono/chains
9	6.74	998, 1040	296	T_d, mono/chains + O_h
18.3	28	998, 1040	290−370, 470 (sh)	T_d, mono/chains + O_h
21.9	36	998, 1040	428, 270, 355, 481 (sh)	T_d, mono/chains + O_h

attributed to stretching and bending modes of V−O bonds, as a series of bands in this region is visible for $OV[OSi(O^tBu)_3]_3$. The band at ~681 cm^{-1} can also be assigned to stretching motions of oxygen in a bridging position between three vanadium atoms (OV_3), by comparison with previous results.[37] These results therefore suggest that the weak band at 684 cm^{-1} observed for the 7.2 wt % of V sample is related to a small number of vanadia ribbons. The sharp band at 1035 cm^{-1} is characteristic of the V═O stretching vibration of tetrahedral VO_4 species.[13,15−18,36] Its formation demonstrates that dehydration changes the molecular structure of the surface vanadia species significantly, in agreement with previous reports.[16,17] Upon cooling to room temperature the band experiences a blue shift to 1040 cm^{-1} (see spectrum at top). The observed frequency shift is a well-known phenomenon in the Raman spectroscopy of solids and is related to the temperature dependence of the crystal lattice parameters.[38] The Raman bands at 915 and 1078 cm^{-1} are characteristic of Si−O^- and Si($-O^-$)$_2$ functionalities,[39] which have been assigned to perturbed silica vibrations that are indicative of the formation of V−O−Si bonds.[18]

4. Spectroscopic Characterization of VO_x/SBA-15. After calcination, the supported vanadium oxide species can be present in several VO_x structures such as isolated tetrahedral VO_4 species, polymeric surface species, and crystalline V_2O_5. Raman and UV−vis diffuse reflectance spectroscopy were used to elucidate the structure of SBA-15-supported vanadia species. The results are summarized in Table 2.

Figure 4 depicts Raman spectra of dehydrated vanadia samples as a function of loading. At low loadings (<9 wt % of V), the spectra are dominated by a strong band at 1040 cm^{-1}, which is characteristic for the V═O stretching vibration of tetrahedral VO_4 species.[15,17−20] The intensity of the 1040-cm^{-1} band increases with loading. When the loading reaches ~9 wt

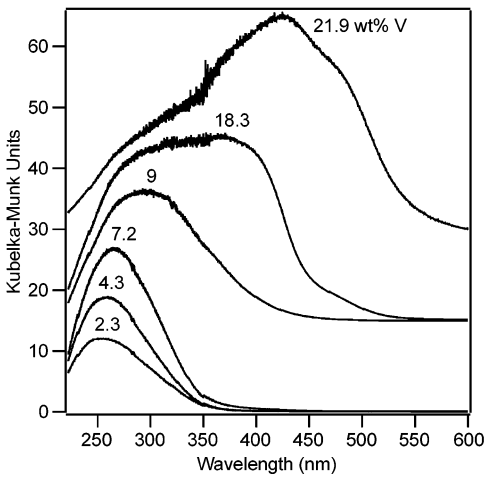

Figure 5. UV−vis diffuse reflectance spectra of dehydrated SBA-15-supported vanadia samples. To more easily compare the absorption changes, the spectra at 9 and 18.3 wt % are set to a baseline of 15 K-M units and the spectrum at 21.9 wt % is set to a baseline of 30 K-M units.

% V, an additional band appears at 998 cm^{-1}, which is attributed to crystalline V_2O_5. These results indicate that at this loading (∼9 wt % of V) vanadium centers aggregate to form crystallites of V_2O_5 that can be observed by Raman spectroscopy.

At high loadings (>9 wt %), the strong 998-cm^{-1} band dominates the spectra and strongly increases with loading. Recently, the ratio of scattering cross-sections for bulk V_2O_5 and isolated tetrahedral VO_4 has been estimated to be 10.[17] Using this ratio of Raman cross-sections and assuming that only V_2O_5 crystallites and isolated VO_4 species are present, the ratio of V_2O_5:VO_4 for the 9, 18.3, and 21.9 wt % of V sample is estimated to be 0.05, 0.36, and 0.39, respectively.

The VO_x concentrations at which V_2O_5 is observed (>2.3 V/nm^2, see Table 2) are well below those required for a monolayer of polymeric vanadia (∼10 V/nm^2), calculated on the basis of the literature value for the cross-sectional area of a $VO_{5/2}$ group of 0.103 nm^2.[40] This indicates that the VO_x surface species tend to form larger clusters, when a certain VO_x concentration is reached. Recently, a similar behavior has been observed for MCM-48-supported vanadia, although the formation of crystalline V_2O_5 was observed at even lower concentrations (<0.63 V/nm^2) compared to VO_x/SBA-15.[7] However, similar dispersions as in the present study have been obtained by multiple impregnation (2.6 V/nm^2)[18] or gas-phase deposition (2.3 V/nm^2)[41] of vanadium isopropoxide onto amorphous silica.

Additional structural information on the surface VO_x species can be obtained from UV−vis diffuse reflectance measurements. It is known that the energy of the oxygen → vanadium charge-transfer bands (CT bands) serves as a good indicator for the coordination of the central V^{5+} center. In general, with increasing coordination number a shift in the CT band to lower energy (higher wavelength) is observed.[7,15,18] UV−vis diffuse reflectance spectra of dehydrated SBA-15-supported vanadia samples are shown in Figure 5. For clarity, the baseline of the spectra for the 9 and 18.3 wt % sample were set to 15 Kubelka−Munk (K-M) units and the spectrum of the 21.9 wt % sample is set to a baseline of 30 K-M units. Their absorption band maxima are summarized in Table 2. Clearly, a red shift of the longest wavelength CT band with increasing vanadium loading is observed. As discussed in the following, a comparison of the band maxima of our data (Table 2) and those of vanadium reference compounds allows us to assign the molecular structures of vanadia on SBA-15 more accurately.[36,42−49] The model compound $OV[OSi(O^tBu)_3]_3$ was measured to have an absorption maximum at 250 nm.[36] In Na_3VO_4 and $Mg_3V_2O_8$ the monomeric vanadium ion is tetrahedrally coordinated with band maxima at 253/294 nm and 260/303 nm, respectively.[46,48,49] $Mg_2V_2O_7$ consists of chains of edge-sharing V_2O_7 groups, and the V_2O_7 groups are composed of corner-sharing tetrahedral VO_4 units.[46,47] Its CT band is found at 280 nm. NH_4VO_3 and $NaVO_3$ both consist of polymerized VO_4 units and give rise to band maxima at 288/363 and 281/353 nm, respectively.[45,44] In crystalline V_2O_5, vanadium is located in the center of a distorted octahedron. The band maximum at 481 nm is responsible for the orange color of the oxide.[42,43] It becomes clear from these data that the position of the longest wavelength CT band strongly depends on the coordination number of the central vanadium ion. This CT band shows a red shift when coordination of the vanadium cation changes from tetrahedral to square pyramidal to octahedral.

In the present study, a very similar absorption behavior is observed for loadings of up to 7.2 wt % of V. As discussed below, two bands are found at 250 and 292 nm. Their intensity increases nearly linearly with VO_x loading. On the basis of the Raman band at 1040 cm^{-1} (see Figure 4), they are assigned to isolated tetrahedral VO_4 species. Moreover, the position of their band maxima is in good agreement with those of reference compounds for isolated VO_4. The samples with V loadings above 7.2 wt % give rise to additional absorption bands between 300 and 400 nm, indicating the presence of polymerized VO_4. Besides, V_2O_5 crystallites are found, as evidenced by Raman. At the highest V loading (21.9 wt %), strong absorption above 400 nm suggests the presence of a larger fraction of V_2O_5 crystallites, in agreement with the intensity increase of the Raman band at 998 cm^{-1}.

At high surface densities of isolated VO_4 monomers, condensation may lead to the formation of polymers. To determine the structure of the surface vanadia species in more detail, the spectra of the samples up to 7.2 wt % have been deconvoluted. As a result, a set of bands (with Gaussian line shape) is obtained for each UV−vis spectrum (see Figure 6). The data in Figure 6 can be described on the basis of three different CT bands with absorption maxima at 250, 292, and 362 nm, respectively. Up to a loading of 4.3 wt %, two bands are found at 250 and 292 nm whose intensity increases with VO_x loading. For the 7.2 wt % sample, an additional charge-transfer band appears at 362 nm. By comparison with reference compounds, the band at 362 nm indicates the presence of some polymerized VO_4 tetrahedra, but their contribution to the total intensity is small.

5. Molecular Structures of Dehydrated SBA-15-Supported VO_x. Spectroscopic characterization of SBA-15-supported VO_x as a function of loading, using Raman and UV−vis spectroscopy, reveals the presence of different VO_x surface structures (Scheme 2). At low vanadia loadings (<7.2 wt %), the surface is exclusively covered by isolated tetrahedral VO_4 species (a, b), while at higher loadings (7.2 wt %), besides isolated tetrahedral, chains of linked tetrahedra are present (c). At vanadia loadings >7.2 wt %, V_2O_5 crystallites are also observed. The structures given in Scheme 2 can be compared with those previously proposed for highly dispersed vanadium oxides on silica prepared by chemical vapor deposition (CVD) of $VO(OC_2H_5)_3$.[16] According to Inumaru et al., using CVD, vanadium oxide thin overlayers, which contain V−O−V bonds, are formed over a wide range of vanadia loadings (0−7.9 wt % of V). In comparison, for our VO_x/SBA-15 samples prepared by grafting/anion exchange, spectroscopic characterization indicates the

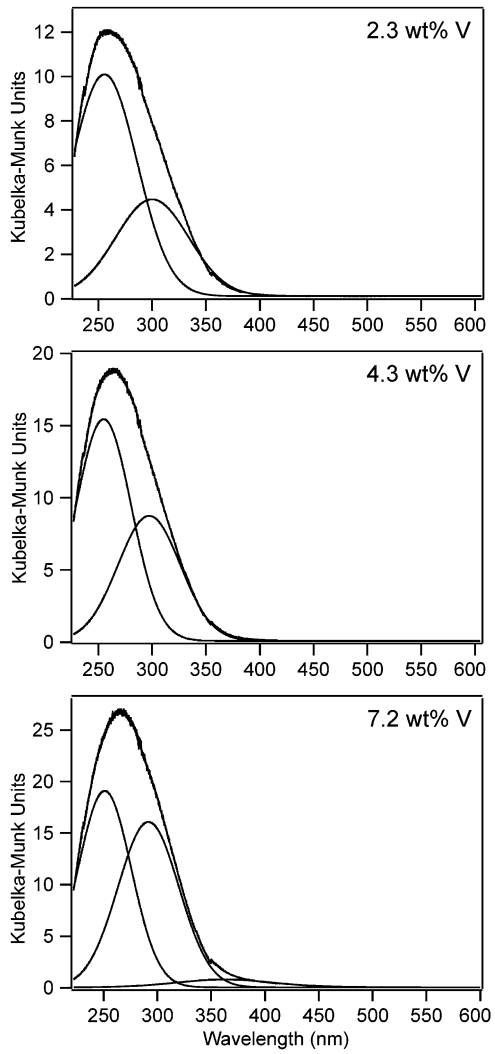

Figure 6. UV−vis diffuse reflectance spectra of dehydrated VO_x/SBA-15 samples at low V loadings together with the results from the deconvolution.

SCHEME 2: Proposed Structural Motifs for Vanadia Supported on Silica

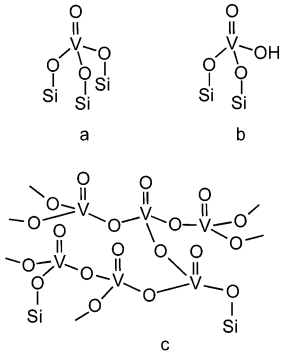

presence of polymeric species only at high loadings (7.2 wt % of V) and in small concentration.

Recently, the OH concentration of SBA-15 (which had been calcined at 500 °C) was determined to be 1.07 OH/nm^2.[50] This value can be considered as a lower limit for the actual OH surface concentration in the SBA-15 samples used for the grafting/ion-exchange of VO_x, as they were used without any temperature pretreatment. According to Zhuravlev, the silanol concentration of a fully hydroxylated silica surface amounts to 4.6 ± 0.5 OH/nm,[2,51] which is claimed to be independent of the origin and characteristics (such as specific surface area, type of pores, pore size distribution) of the sample. Raman spectroscopy shows that surface Si−OH hydroxyls are consumed during deposition of 7.2 wt % of V (2.3 V/nm^2). Anchoring of these V atoms by formation of three-legged VO_4 species requires an OH surface concentration of ($3 \times 2.3 = 6.9$) OH/nm^2. Therefore, some Si−O−Si siloxane bridges must be broken during the dehydration process, as evidenced by the Raman results (see Figure 3).

Conclusions

SBA-15-supported vanadium oxide species have been prepared by a grafting/anion exchange method, which includes (1) functionalization of the inner pores of SBA-15 with 3-aminopropyltrimethoxysilane, (2) ion-exchanging decavanadate into the pores, and (3) decomposition of the decavanadate precursor to yield highly dispersed vanadia. Using this approach, vanadium loadings of up to 22 wt % of V on SBA-15 were obtained. The experimental maximum dispersion of VO_x/SBA-15 was achieved at ~7.2 wt % of V (2.3 V/nm^2). Using visible Raman spectroscopy, various steps of the synthesis were studied. On the basis of these and previous spectroscopic results, a reaction mechanism for the formation of VO_x/SBA-15 is proposed.

Raman spectra recorded during dehydration of VO_x/SBA-15 show dramatic changes in the molecular structure of the surface vanadia species. Spectroscopic characterization of the dehydrated supported vanadia species by Raman and UV−vis diffuse reflectance spectroscopy shows the presence of different VO_x structures as a function of loading. Below 7.2 wt % of V, the surface is exclusively covered with isolated tetrahedral VO_4 species. At higher vanadia loadings (7.2 wt %), a small fraction of chains of linked tetrahedra is present besides VO_4 monomers. To provide the necessary surface OH concentration for the formation of the isolated VO_4 species at 7.2 wt %, Si−O−Si siloxane bridges have to be broken. At V loadings above 7.2 wt %, besides monomers and polymers, V_2O_5 crystallites are found. Their fraction increases with vanadium loading, ultimately up to 40% of that of VO_4 at 21.9 wt % of V.

Acknowledgment. The authors thank Gabor Somorjai and Peidong Yang for helpful discussions, and Joel Ager for performing X-ray diffraction measurements. This work was supported by the Director, Office of Energy Research, Office of Basic Energy Sciences, Chemical Sciences Division, of the U.S. Department of Energy under Contract No. DE-AC03-76SF00098. C.H. thanks the Max-Planck Society for providing a fellowship.

References and Notes

(1) Zhao, D. Y.; Feng, J. L.; Huo, Q. S.; Melosh, N.; Fredrickson, G. H.; Chmelka, B. F.; Stucky, G. D. *Science* **1998**, *279*, 548.

(2) Cassiers, K.; Linssen, T.; Mathieu, M.; Benjelloun, M.; Schrijnemakers, K.; Van der Poort, P.; Cool, P.; Vansant, E. F. *Chem. Mater.* **2002**, *14*, 2317.

(3) Jarupatrakorn, J.; Tilley, T. D. *J. Am. Chem. Soc.* **2002**, *124*, 8380.

(4) Liu, Y.-M.; Cao, Y.; Zhu, K.-K.; Yan, S.-R.; Dai, W.-L.; He, H.-Y.; Fan, K.-N. *Chem. Commun.* **2002**, 2832.

(5) Lopez, H. H.; Martinez, A. *Catal. Lett.* **2002**, *83*, 37.

(6) Carvalho, W. A.; Wallau, M.; Schuchardt, U. *J. Mol. Catal. A* **1999**, *144*, 91.

(7) Baltes, M.; Cassiers, K.; Van der Voort, P.; Weckhuysen, B. M.; Schoonheydt, R. A.; Vansant, E. F. *J. Catal.* **2001**, *197*, 160 and references therein.

(8) Sun, Q.; Jehng, J. M.; Hu, H. H.; Herman, R. G.; Wachs, I. E.; Klier, K. J. *J. Catal.* **1997**, *165*, 91.

(9) Irusta, S.; Cornaglia, L. M.; Miro, E. E.; Lombardo, E. A. *J. Catal.* **1995**, *156*, 167.

(10) Kim, D. S.; Tatibouet, J. A.; Wachs, I. E. *J. Catal.* **1992**, *136*, 209.

(11) Deo, G.; Wachs, I. E.; Haber, J. *Crit. Rev. Surf. Chem.* **1994**, *40*, 1.

(12) Jeng, J.-M.; Hu, H.; Gao, X.; Wachs, I. E. *Catal. Today* **1996**, *28*, 335.

(13) Banares, M.; Gao, X.; Fierro, J. L. G.; Wachs, I. E. *Stud. Surf. Sci. Catal.* **1997**, *110*, 295.

(14) Johnson, B.; Rebenstrof, B.; Larsson, R.; Andersson, S. L. *J. Chem. Soc., Faraday Trans. 1* **1988**, *84*, 1897.

(15) (a) Schraml-Marth, M.; Wokaun, A.; Pohl, M.; Krauss, H. L. *J. Chem. Soc., Faraday Trans.* **1991**, *87*, 2635. (b) Scharf, U.; Schraml-Marth, M.; Wokaun, A.; Baiker, A. *J. Chem. Soc., Faraday Trans.* **1991**, *87*, 3299.

(16) (a) Inumaru, K.; Okuhara, T.; Misono, M.; Matsubayashi, N.; Shimada, H.; Nishijima, A. *J. Chem. Soc., Faraday Trans.* **1992**, *88*, 625. (b) Inumaru, K.; Okuhara, T.; Misono, M. *J. Phys. Chem.* **1991**, *95*, 4826. (c) Inumaru, K.; Misono, M.; Okuhara, T. *Appl. Catal. A* **1997**, *149*, 133.

(17) Xie, S.; Iglesia, E.; Bell, A. T. *Langmuir* **2000**, *16*, 7162.

(18) Gao, X.; Bare, S. R.; Weckhuysen, B.; Wachs, I. E. *J. Phys. Chem. B* **1998**, *102*, 10842.

(19) Das, N.; Eckert, H.; Hu, H.; Wachs, I. E.; Walzer, J. F.; Feher, F. J. *J. Phys. Chem.* **1993**, *97*, 8240.

(20) Went, G. T.; Oyama, S. T.; Bell, A. T. *J. Phys. Chem.* **1990**, *94*, 4240.

(21) Roozeboom, F.; Mittelmeljer-Hazeleger, M. C.; Mouljin, J. A.; Medema, J.; de Beer, V. H. J.; Gellings, P. J. *J. Phys. Chem.* **1980**, *84*, 2783.

(22) Lische, G.; Hanke, W.; Jerschkewitz, H. G.; Ohlmann, J. *J. Catal.* **1985**, *91*, 54.

(23) Arena, F.; Frusteri, F.; Martra, G.; Coluccia, S.; Parmaliana, A. *J. Chem. Soc., Faraday Trans.* **1997**, *93*, 3849.

(24) (a) Yoshida, S.; Tanaka, T.; Nishimura, Y.; Mizutani, H.; Funabiki, T. *Proc. 9th Int. Congr. Catal.* **1988**, *3*, 1473. (b) Yoshida, S.; Tanaka, T.; Hanada, T.; Hiraiwa, T.; Kanai, H.; Funabiki, T. *Catal. Lett.* **1992**, *12*, 277. (c) Tanaka, T.; Yamashita, H.; Tsuchitani, R.; Funabiki, T.; Yoshida, S. *J. Chem. Soc., Faraday Trans.* **1988**, *84*, 2987.

(25) Vrancken, K. C.; Van Der Voort, P.; Possemiers, K.; Vansant, E. F. *J. Colloid Int. Sci.* **1995**, *174*, 86.

(26) Roman, P.; Aranzabe, A.; Luque, A.; Gutierrez-Zorilla, J. M. *Mater. Res. Bull.* **1991**, *26*, 731.

(27) Brunauer, S.; Emmett, P. H.; Teller, E. *J. Am. Chem. Soc.* **1938**, *60*, 309.

(28) Barret, E. P.; Joyner, L. G.; Halenda, P. P. *J. Am. Chem. Soc.* **1951**, *73*, 373.

(29) Brinker, C. J.; Kirkpatrick, R.; Tallant, D. R.; Bunker, B. C.; Montez, B. *J. Non-Cryst. Solids* **1988**, *99*, 418.

(30) (a) Tallant, D. R.; Bunker, B. C.; Brinker, C. J.; Balfe, C. A. *Mater. Res. Soc. Symp. Proc.* **1986**, *73*, 261. (b) Stolen, R. H.; Walrafen, G. E. *J. Chem. Phys.* **1976**, *64*, 2623. (c) Brinker, B. C.; Tallant, D. R.; Roth, E. P.; Ashley, C. S. *Mater. Res. Soc. Symp. Proc.* **1986**, *61*, 387.

(31) Lin-Vien, D.; Colthup, N. B.; Fateley, W. G.; Grasselli, J. G. *The Handbook of Infrared and Raman Characteristic Frequencies of Organic Molecules*; Academic Press: Boston, MA, 1991.

(32) Hardcastle, F. D.; Wachs, I. E. *J. Phys. Chem.* **1991**, *95*, 5031.

(33) (a) Abello, L.; Husson, E.; Repelin, Y.; Lucazeau, G. *J. Solid State Chem.* **1985**, *56*, 379. (b) Repelin, Y.; Husson, E.; Abello, L.; Lucazeau, G. *Spectrochim. Acta* **1985**, *41A*, 993.

(34) Previous studies on amorphous silica have shown that the APTS molecules are predominantly in their bidentate/tridentate form.[35] Based on steric reasons it was concluded that three covalent bonds with the surface can be excluded implying polymerization of tridentate APTS.

(35) Vansant, E. F.; Van Der Voort, P.; Vrancken, K. C. *Characterization and Chemical Modification of the Silica Surface*; Elsevier: Amsterdam, The Netherlands, 1995.

(36) Rulkens, R.; Male, J. L.; Terry, K. W.; Olthof, B.; Khodakov, A.; Bell, A. T.; Iglesia, E.; Tilley, T. D. *Chem. Mater.* **1999**, *11*, 2966.

(37) Walther, K. L.; Schraml-Marth, M.; Wokaun, A.; Baiker, A. *Catal. Lett.* **1990**, *4*, 327.

(38) Ishii, Y.; Nagasaki, T.; Igawa, N.; Watanabe, H.; Ohno, H. *J. Am. Ceram. Soc.* **1991**, *74*, 2324.

(39) McMillan, P. *Am. Mineral.* **1986**, *69*, 622.

(40) Van Hengstum, A. J.; Van Ommen, J. G.; Bosch, H.; Gellings, P. J. *Appl. Catal.* **1983**, *5*, 207.

(41) Keranen, J.; Guimon, C.; Iiskola, E.; Auroux, A.; Niinisto, L. *J. Phys. Chem. B* **2003**, *107*, 10773.

(42) Wright, A. C. *Philos. Mag. B* **1984**, *50*, L23.

(43) Centi, G.; Perathoner, S.; Trifiro, F.; Aboukais, A.; Aissi, C. F.; Guelton, M. *J. Phys. Chem.* **1992**, *96*, 2617.

(44) Marumo, F.; Isobe, M.; Iwai, S.; Kondo, Y. *Acta Crystallogr.* **1974**, *B30*, 1628.

(45) Evans, H. T. *Z. Krystallogr.* **1960**, *114*, 257.

(46) (a) Sam, D. S. H.; Soenen, V.; Volta, J. C. *J. Catal.* **1990**, *123*, 417. (b) Busca, G.; Ricchiardi, G.; Sam, D. S. H.; Volta, J. C. *J. Chem. Soc., Faraday Trans.* **1994**, *90*, 1161.

(47) Gopal, R.; Calvo, C. *Acta Crystallogr.* **1974**, *B30*, 2491.

(48) Krishnamachari, N.; Calvo, C. *Can. J. Chem.* **1971**, *49*, 1629.

(49) Nabavi, M.; Taulelle, F.; Sanchez, C.; Verdaguer, M. *J. Phys. Chem. Solids* **1990**, *51*, 1375.

(50) Fujdala, K. L.; Tilley, T. D. *J. Am. Chem. Soc.* **2001**, *123*, 10133.

(51) (a) Zhuravlev, L. T. *Langmuir* **1987**, *3*, 316. (b) Zhuravlev, L. T. *Colloids Surf. A* **1993**, *74*, 71.